

Kinetics of Thermal Decomposition and Kinetics of Substitution Reaction of Nano Uranyl Schiff Base Complexes

ZAHRA ASADI,¹ AZADE ZEINALI,¹ MICHAL DUSEK,³ VACLAV EIGNER^{2,3}

¹Chemistry Department, College of Sciences, Shiraz University, Shiraz 71454, Iran

²Department of Solid State Chemistry, Institute of Chemical Technology, 166 28, Prague, Czech Republic

³Institute of Physics ASCR, 182 21, Praha, Czech Republic

Received 2 April 2014; accepted 3 September 2014

DOI 10.1002/kin.20881

Published online 15 October 2014 in Wiley Online Library (wileyonlinelibrary.com).

ABSTRACT: This study focuses on the synthesis, characterization, and kinetics of substitution reaction of new uranyl Schiff base complexes prepared in a crystalline state as well as in a form of nanoparticles with sizes ranging between 35 and 60 nm. Preliminary Fourier transform infrared spectroscopy (FTIR) and thermogravimetric (TG) measurements indicated no difference between the two forms. The compounds were characterized by UV–vis, ¹H NMR, cyclic voltammetry, X-ray crystallography, FTIR, TG, and CHN analyses. X-ray crystallography revealed coordination of the uranyl by the tetradentate Schiff base ligand and one solvent molecule, resulting in seven-coordinated uranium. Cyclic voltammetry of the complexes in acetonitrile revealed the quasi-reversible redox reaction. The TG and analysis of Coats–Redfern plots revealed that the kinetics of thermal decomposition of the complexes is of the first order in all stages. The study of the kinetics and the mechanism of the exchange reaction of the coordinated solvent with tributylphosphine was performed by the spectrophotometric method. The second-order rate constants at four temperatures and the activation parameters revealed an associative mechanism for all corresponding complexes. Anticancer activity of the nano uranyl Schiff base complexes against cancer cell lines (Jurkat) was studied and determined by the MTT (3-[4,5-dimethylthiazol-2-yl]-2,5-diphenyl-tetrazoliumbromide) assay. © 2014 Wiley Periodicals, Inc. *Int J Chem Kinet* 46: 718–729, 2014

Correspondence to: Z. Asadi; e-mail: zasadi@shirazu.ac.ir, zasadi@susc.ac.ir

Contract grant sponsor: Shiraz University Research Council.
Supporting Information is available in the online issue at www.wileyonlinelibrary.com.

© 2014 Wiley Periodicals, Inc.

INTRODUCTION

Since the beginning of this century, the interest in materials at the nanoscale has been steadily increasing based on the fact that the quantum size of nanomaterials

triggers new physical, electronic, and magnetic properties. Thus the synthesis and characterization of nanostructures with different particle sizes and morphologies are important both from the viewpoint of basic science as well as for technological applications [1–3]. A few studies have been done on the synthesis of nanoparticles of Schiff base complexes and their application [4].

In this paper, efforts were taken on the synthesis of three new uranyl Schiff base complexes (Fig. S1 in the Supporting Information), their characterization, and preparation in the form of nanoparticles. X-ray crystallography and thermogravimetry revealed that one-solvent molecule coordinates weakly to the uranium center in comparison with the Schiff base and *trans* oxides. We also studied kinetics of exchange of this solvent molecule with tributylphosphine.

EXPERIMENTAL

Chemicals and Apparatus

2-Hydroxysalicylaldehyde, 5-chloro-2-hydroxysalicylaldehyde, 2-hydroxysalicylaldehyde, 2-aminobenzylamine, uranylacetate dihydrate $\text{UO}_2(\text{OAc})_2 \cdot 2\text{H}_2\text{O}$, tri-*n*-butylphosphine (PBu_3), chloroform (CHCl_3), methanol, DMSO- d_6 for ^1H NMR spectroscopy, acetonitrile (CH_3CN), and potassium bromide (KBr) for IR spectroscopy, were purchased from Merck, Acros, and Aldrich.

The electronic absorption spectra were recorded using a Perkin–Elmer Lambda 2 spectrophotometer equipped with a Lauda-ecoline-RE 104 thermostat. Fourier transform infrared spectroscopy (FTIR) spectra were recorded on a Shimadzu FTIR–8300 infrared spectrophotometer. The ^1H NMR spectra were recorded on a Bruker Advance DPX–250 spectrometer at 250 MHz. Elemental microanalyses (CHN) were obtained using a CHN Thermo-Fining Flash EA1112 analyzer. A Buchi 535 instrument was used to obtain the melting point of the compounds. Thermal gravimetric analyses were recorded on a Perkin–Elmer Pyris Diamond model. Electrochemical studies were carried out using an Auto lab 302N instrument. A three-electrode system was utilized with a glassy carbon working electrode, a reference electrode (Ag/Ag^+ in tetrabutylammoniumperchlorate (TBAP)/acetonitrile solution), and a Pt auxiliary electrode. The measurements of cyclic voltammetry (CV) for the CH_3CN solution containing uranyl complexes (1.00×10^{-3} M, $M = \text{mol}/\text{dm}^3$) and TBAP (0.10 M)

were carried out in the potential ranging from 0.2 to –1.4 V. TBAP was used as a supporting electrolyte. An incubator and an ELISA reader (Bio-Tek's ELx808, USA) were used for anticancer studies. Transmission electron microscopy (TEM) images were obtained on a Zeiss EM10C transmission electron microscope using the Acc voltage of 60 kV.

Synthesis of the Schiff Base Ligands

Schiff bases were synthesized by the condensation of 2-aminobenzylamine (1 mmol) with substituted salicylaldehyde (2 mmol) in methanol. The purity of the ligands was checked by the thin-layer chromatography. The solution was refluxed for 6–7 h (Scheme S1 in the Supporting Information). The Schiff base ligand was precipitated by cooling and washed with small amounts of cold methanol (5 mL) and diethylether (5 mL).

N,N'-bis(salicylidene)-2-aminobenzylamine (H_2salbz): Yield: 62.8%, color: yellow, mp = 106°C , Anal. Found (Calcd.): $\text{C}_{21}\text{H}_{18}\text{N}_2\text{O}_2$ (330.21): C, 76.54 (76.34); H, 5.43(5.49); N, 8.40(8.48). IR (KBr, cm^{-1}): 3423 ($\nu_{\text{O-H}}$), 3042 ($\nu_{\text{C-H}}$), 1633, 1619 ($\nu_{\text{C=N}}$), 1570–1442 ($\nu_{\text{C=C}}$). ^1H NMR (250 MHz, DMSO- d_6 , room temperature): δ (ppm) = 4.95 (s, 2H, CH_2), 6.84–7.41 (m, 12H, ArH), 8.47 (s, 1H^(a), HC=N), 8.58 (s, 1H^(b), HC=N), 13.28, 13.51 (s, 2H, OH). UV–vis.(acetonitrile): λ_{max} (nm), ϵ ($\text{M}^{-1} \text{cm}^{-1}$) = 212 (~79,599), 256 (~41,700), 404 (~24,643).

N,N'-bis(5-chlorosalicylidene)-2-aminobenzylamine (5-Cl salbzH_2): Yield: 84%, color: yellow, mp = 127°C , Anal. Found (Calcd.): $\text{C}_{21}\text{H}_{16}\text{Cl}_2\text{N}_2\text{O}_2$ (399.11): C, 63.23 (63.17); H, 3.86 (4.04); N, 7.18 (7.02). IR (KBr, cm^{-1}): 3456 ($\nu_{\text{O-H}}$), 2883 ($\nu_{\text{C-H}}$), 1633, 1614 ($\nu_{\text{C=N}}$), 1556–1474 ($\nu_{\text{C=C}}$). ^1H NMR (250 MHz, DMSO- d_6 , room temperature): δ (ppm) = 4.93 (s, 2H, CH_2), 6.85–7.52 (m, 10H, ArH), 8.37 (s, 1H^(a), HC=N), 8.50 (s, 1H^(b), HC=N), 13.19, 13.41 (s, 2H, OH). UV–vis.(acetonitrile): λ_{max} (nm), ϵ ($\text{M}^{-1} \text{cm}^{-1}$) = 223 (~96178), 260 (~62,685), 332 (~21,073).

N,N'-bis(5-boromosalicylidene)-2-aminobenzylamine (5-Br SalbzH_2): Yield: 87.9%, color: yellow, mp = 145.3°C , Anal. Found (Calcd.): $\text{C}_{21}\text{H}_{16}\text{Br}_2\text{N}_2\text{O}_2$ (488.01): C, 51.65(51.67); H, 3.33(3.30); N, 5.90(5.74). IR (KBr, cm^{-1}): 3436 ($\nu_{\text{O-H}}$), 3058–2883 ($\nu_{\text{C-H}}$), 1633, 1604 ($\nu_{\text{C=N}}$), 1556–1469 ($\nu_{\text{C=C}}$), ^1H NMR (250 MHz, DMSO- d_6 , room temperature): δ (ppm) = 4.96 (s, 2H, CH_2), 6.80–7.49 (m, 10H, ArH), 8.35 (s, 1H^(a), HC=N), 8.49 (s, 1H^(b), HC=N), 12.99, 13.21 (s, 2H, OH). UV–vis. (acetonitrile): λ_{max} (nm), ϵ ($\text{M}^{-1} \text{cm}^{-1}$) = 222 (~83,803), 257 (sh), 330 (~17,538).

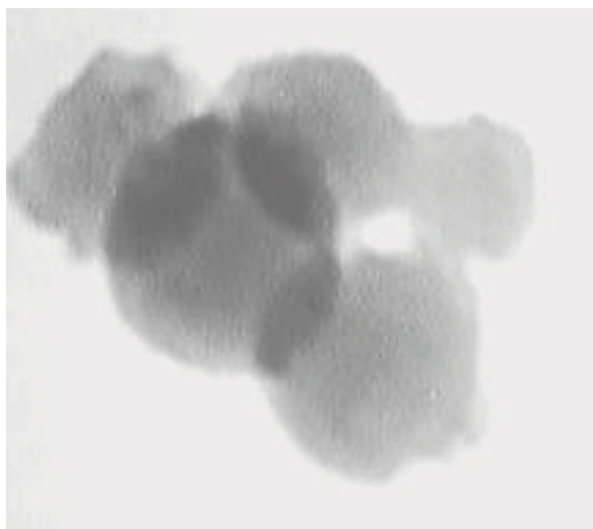


Figure 1 TEM image of nanoparticles of $[\text{UO}_2(5\text{-Brsalbz})(\text{MeOH})]$ with sizes ranging between 35 and 60 nm.

Synthesis of Nano Uranyl Schiff Base Complexes

Nano uranyl complexes were prepared by slow addition of uranyl acetate, dissolved in 50 mL methanol, into a hot methanolic solution of ligand (1:1 molar ratio). The mixture was then refluxed for 24 h (Scheme S2 in the Supporting Information). The precipitated solid was filtered and washed with methanol and ether. TEM images showed that nanoparticles with different sizes range between 35 and 60 nm (Fig. 1).

$[\text{UO}_2(\text{salbz})(\text{MeOH})]$ Yield: 92%, Color: dark orange, mp $>250^\circ\text{C}$, Anal. Found (Calcd.): $\text{C}_{22}\text{H}_{20}\text{N}_2\text{O}_5\text{U}$ (630.22): C, 41.26 (41.36); H, 3.66 (3.71); N, 4.17 (4.19). IR (KBr, cm^{-1}): 3436 ($\nu_{\text{O-H}}$), 2932–3262 ($\nu_{\text{C-H}}$), 1590, 1612 ($\nu_{\text{C=N}}$), 1537 ($\nu_{\text{C=C}}$), 906 ($\nu_{\text{U=O}}$), 756.5 ($\nu_{\text{U-N}}$), 592.6 ($\nu_{\text{U-O}}$). ^1H NMR (250 MHz, DMSO- d_6 , room temperature): δ (ppm) = 3.14 (d, 3H, MeOH), 4.07 (q, 1H, MeOH), 5.32 (s, 2H, CH_2), 6.65–7.80 (m, 12H, ArH), 9.28 (s, 1H^(a), HC=N), 9.57 (s, 1H^(b), HC=N). UV-vis. (acetonitrile): λ_{max} (nm), ϵ ($\text{M}^{-1}\text{cm}^{-1}$) = 231 ($\sim 65,565$), 267 (sh), 329 ($\sim 15,114$), 397 (sh).

$[\text{UO}_2(5\text{-Clalsalbz})(\text{MeOH})]$ Yield: 88%, Color: orange, mp $>250^\circ\text{C}$, Anal. Found (Calcd.): $\text{C}_{22}\text{H}_{18}\text{Cl}_2\text{N}_2\text{O}_2\text{U}$ (699.12): C, 38.55 (38.79); H, 2.78 (2.59); N, 4.29 (4.01). IR (KBr, cm^{-1}): 3294 ($\nu_{\text{O-H}}$), 2831–3039 ($\nu_{\text{C-H}}$), 1590, 1612 ($\nu_{\text{C=N}}$), 1458–1535 ($\nu_{\text{C=C}}$), 902 ($\nu_{\text{U=O}}$), 702 ($\nu_{\text{U-N}}$), 648 ($\nu_{\text{U-O}}$). ^1H NMR (250 MHz, DMSO- d_6 , room temperature): δ (ppm) = 3.14 (d, 3H, MeOH), 4.09 (q, 1H, MeOH), 5.33 (s, 2H, CH_2), 6.92–7.89 (m, 10H, ArH), 9.28 (s, 1H^(a),

HC=N), 9.56 (s, 1H^(b), HC=N). UV-vis. (acetonitrile): λ_{max} (nm), ϵ ($\text{M}^{-1}\text{cm}^{-1}$) = 234 ($\sim 73,360$), 340 ($\sim 13,218$), 404 (sh).

$[\text{UO}_2(5\text{-Brsalbz})(\text{MeOH})]$ Yield: 91.7%, Color: orange, mp $>250^\circ\text{C}$, Anal. Found (Calcd.): $\text{C}_{22}\text{H}_{18}\text{Br}_2\text{N}_2\text{O}_5\text{U}$ (788.02): C, 33.34 (33.52); H, 2.10 (2.30); N, 3.63 (3.55). IR (KBr, cm^{-1}): 3340 ($\nu_{\text{O-H}}$), 2923–3047 ($\nu_{\text{C-H}}$), 1585, 1612 ($\nu_{\text{C=N}}$), 1458–1527 ($\nu_{\text{C=C}}$), 894 ($\nu_{\text{U=O}}$), 686 ($\nu_{\text{U-N}}$), 640 ($\nu_{\text{U-O}}$). ^1H NMR (250 MHz, DMSO- d_6 , room temperature): δ (ppm) = 3.14 (d, 3H, MeOH), 4.08 (q, 1H, MeOH), 5.32 (s, 2H, CH_2), 6.87–7.99 (m, 10H, ArH), 9.27 (s, 1H^(a), HC=N), 9.56 (s, 1H^(b), HC=N). UV-vis. (acetonitrile): λ_{max} (nm), ϵ ($\text{M}^{-1}\text{cm}^{-1}$) = 235 ($\sim 71,208$), 340 ($\sim 13,218$), 404 (sh).

Kinetic Studies of the Substitution Reactions

The kinetics of exchange reactions on the uranyl center was studied. Kinetic data were determined spectrophotometrically. In all cases (runs from 10.0 to $-40.0 \pm 0.1^\circ\text{C}$), the procedure involved adding a sample of PBU_3 under the pseudo-first-order condition to a solution containing the uranyl complex. The kinetics was followed at a predetermined wavelength, where the difference in the absorption between the substrate and the product was the largest. After each injection, the absorbance was read with definite time intervals.

Synthesis of the Kinetic Product, $[\text{UO}_2(\text{Schiff base})(\text{PBU}_3)]$

The uranyl Schiff base complex, $[\text{UO}_2(5\text{-Brsalbz})(\text{MeOH})]$, was dissolved in methanol (15 mL), and PBU_3 was added gradually with constant stirring. The stoichiometry of the complex to PBU_3 was 1:1. The solution was stirred for 6–7 h. The reaction was carried out at 50°C , under N_2 atmosphere. The precipitate was formed and washed with cold methanol (5 mL) and cold ether (5 mL).

$[\text{UO}_2(5\text{-Brsalbz})(\text{PBU}_3)]$ Yield: 85.2%, Color: orange, mp $>250^\circ\text{C}$, Anal. Found (Calcd.): $\text{C}_{33}\text{H}_{41}\text{Br}_2\text{N}_2\text{O}_4\text{UP}$ (958.11): C, 40.95 (41.37); H, 4.41 (4.53); N, 2.97 (2.85). IR (KBr, cm^{-1}): 3425 ($\nu_{\text{O-H}}$), 2869–2962 ($\nu_{\text{C-H}}$), 1612 ($\nu_{\text{C=N}}$), 1458–1527 ($\nu_{\text{C=C}}$), 902 ($\nu_{\text{U=O}}$), 686 ($\nu_{\text{U-N}}$), 632 ($\nu_{\text{U-O}}$). ^1H NMR (250 MHz, DMSO- d_6 , room temperature): δ (ppm) = 0.85–1.35 (m, 27H, PBU_3), 5.32 (s, 2H, CH_2), 6.86–7.99 (m, 10H, ArH), 9.27 (s, 1H^(a), HC=N), 9.56 (s, 1H^(b), HC=N).

Table I Crystal Data, Data Collection, and Structure Refinement Details for the Complexes

	[UO ₂ (salbz)(DMF)]	[UO ₂ (5-Clalbz)(DMF)]	[UO ₂ (5-Brsalbz)(DMF)]
Formula	C ₂₄ H ₂₃ N ₃ O ₅ U	C ₂₄ H ₂₁ Cl ₂ N ₃ O ₅ U	C ₂₄ H ₂₁ Br ₂ N ₃ O ₅ U
Formula weight	671.5	740.4	829.3
Crystal system	Monoclinic	Monoclinic	Monoclinic
Hall group	<i>C</i> -2yc	- <i>P</i> 2ybc	<i>P</i> 2ybc
Space group	<i>C</i> <i>c</i>	<i>P</i> 21/ <i>c</i>	<i>P</i> 21/ <i>c</i>
<i>T</i> (K)	120	120	120
<i>a</i> (Å)	9.9418(1)	11.5513(3)	11.7171(4)
<i>b</i> (Å)	21.7540(2)	25.4605(6)	25.8147(9)
<i>c</i> (Å)	10.9929(1)	8.4861(2)	8.4127(4)
α (°)	90	90	90
β (°)	107.7472(12)	94.462(2)	94.222(4)
γ (°)	90	90	90
<i>V</i> (Å ³)	2264.34(4)	2488.21(11)	2537.71(17)
<i>Z</i>	4	4	4
<i>D</i> _x (g cm ⁻³)	1.970	1.976	2.171
<i>F</i> (000)	1280.0	1408.0	1552.0
<i>N</i> _{ref}	11633	6823	4507
<i>T</i> _{min} , <i>T</i> _{max}	0.134, 0.512	0.452, 0.800	0.236, 0.658
<i>R</i> (reflections > 3σ)	0.0188(10739)	0.0273(4628)	0.0256(3614)
w <i>R</i> 2 (all reflections)	0.0427(11633)	0.0586(6076)	0.0304(4437)

X-Ray Crystallography

Red single crystals of the uranyl complexes [UO₂(Schiff base)(DMF)] were obtained in good yield from a slow diffusion of diethyl ether into a solution of the metal complex in dimethylformamide (DMF) at room temperature during 10 days. The crystals were intensely colored. The preparation from DMF/Et₂O gave better single crystals compared with the preparation from acetonitrile, which was also attempted. The diffraction data were obtained using the Gemini diffractometer of Agilent Technologies, with Mo K α radiation from a sealed X-ray tube monochromated with a graphite monochromator and collimated with a Mo-Enhance fiber optics collimator. The CCD Atlas was used for the detection. Data processing was done with CrysAlis Pro [5] and the same program was used for the absorption correction based on the crystal shape. The structures were solved by the program Superflip [6] and refined with Jana 2006 [7]. In the complex **1**, the DMF molecule was disordered between two positions with occupancy 0.716(4) and 0.284(4). The DMF has identical shape in both positions because we used a rigid body approach in its refinement. A comparison with the free atomic model confirmed that the introduction of a rigid body has negligible impact on the *R* values. Moreover, we restricted the distances between the oxygen of DMF and uranium to be the same.

Again, the application of this restriction had negligible impact on the *R* values.

All methods of characterization have been summarized in Table S1 in the Supporting Information.

RESULTS AND DISCUSSION

Characterization of the Complexes

Crystal Structure of the Complexes. We determined three single crystal structures, [UO₂(salbz)(DMF)] (**1**), [UO₂(5-Clalbz)(DMF)] (**2**), and [UO₂(5-Brsalbz)(DMF)] (**3**) and deposited them at the Cambridge Crystallographic Data Center with CCDC codes 949282, 949281 and 949395, respectively. Crystallographic data and details of the data collection are listed in Table I. ORTEP views of the complexes are shown in Figs. 2 and 3, and selected bond parameters are listed in Table S2 in the Supporting Information. The compounds **2** and **3** were found to be isotopic.

The geometry around the uranyl atoms in **1–3** was close to pentagonal-bipyramidal with the axial O=U=O moiety, two oxygen atoms, and two nitrogen atoms in the equatorial position and the solvent molecule (DMF) occupying the fifth coordination site

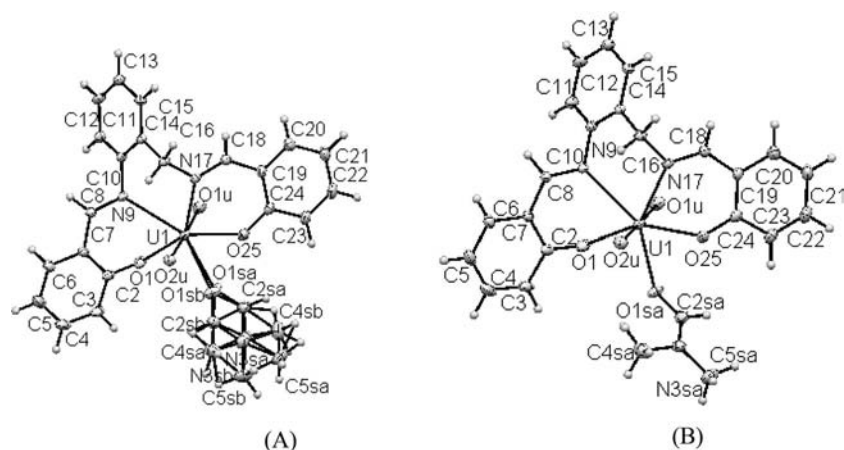


Figure 2 ORTEP view of $[\text{UO}_2(\text{salbz})(\text{DMF})]$ complex. (A) showing disorder of the DMF molecule; (B) showing the more occupied position (78%) of the DMF molecule.

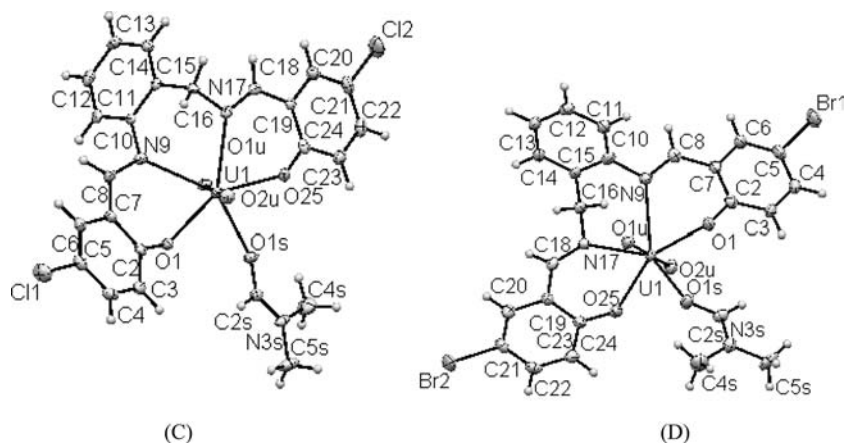


Figure 3 ORTEP view of $[\text{UO}_2(5\text{-Cl-salbz})(\text{DMF})]$ (C) and $[\text{UO}_2(5\text{-Br-salbz})(\text{DMF})]$ (D).

in the equatorial position. In **(1)**, DMF was disordered between two unequally occupied positions (Fig. 2).

The uranyl oxygen distance $\text{U}-\text{O1u}$ in **3** (1.747(4) Å) was slightly shorter than the corresponding distances observed in **1** (1.786(2) Å) and **2** (1.788(3) Å). This trend was almost reverse for $\text{U}-\text{O2u}$ distances; **1** (1.788(2) Å), **2** (1.777(3) Å), and **3** (1.793(4) Å). All these distances were in the range typically found in other reported uranyl Schiff base complexes [8].

The fact that the Schiff bases ligands were asymmetric, resulting in unequal $\text{U}-\text{N}$ distances as well as $\text{U}-\text{O1}$ and $\text{U}-\text{O25}$ distances in all the complexes. For $\text{U}-\text{N9}$ and $\text{U}-\text{N17}$, the distances were 2.640(2) and 2.563(2) Å for **1**, 2.666(3) and 2.559(3) Å for **2**, 2.656(5) and 2.561(5) Å for **3**. The distances $\text{U1}-\text{O1}$ and $\text{U1}-\text{O25}$ were found to be shorter than $\text{U}-\text{N}$ distances and also the difference between them was smaller than the one between $\text{U}-\text{N9}$ and $\text{U}-\text{N17}$. For example, in **3**, $\text{U1}-\text{O1}$

and $\text{U1}-\text{O25}$ was 2.263(4) and 2.228(4) Å, respectively. Such a difference might imply that the coordination of the oxygen atoms in the complexes was stronger than the coordination of the nitrogen atoms. The crystal lattice of the complex contains a DMF molecule, which was the solvent component in the recrystallization. The $\text{U}-\text{O1s}$ distances (2.439(2) Å in **1**, 2.415(3) Å in **2**, and 2.414(4) Å in **3**) were comparable to $\text{U}-\text{O}_{\text{solvent}}$ distances reported for other uranyl complexes [8]. Overall, the bond distance between the oxygen atom of DMF and uranium was longer than those of $\text{U}-\text{O1}$ and $\text{U}-\text{O25}$ in all complexes, suggesting weaker binding of DMF when comparing with the Schiff base.

The $\text{O}=\text{U}=\text{O}$ angles in **2** (175.6(1)°) and **3** (175.8(2)°) indicated that the uranyl moiety was slightly bent compared to the angle observed in **1** (177.1(8)°). These angles also indicated that the uranyl

moiety was slightly bent in the direction opposite to the coordination of DMF. The deviation from linearity was due to the presence of the coordinated solvent.

The coordination geometry around UO_2 was nearly planar with the dihedral angle of $2.56(16)^\circ$ between coordination planes of N17-U1-O24 and N9-U1-O1 . Atoms C10 and C15 belonging to the aromatic rings were out of the equatorial plane, with the distance from the plane $0.449(4)$ Å for C10 and $0.466(4)$ Å for C15. The geometry of hydrogen bonds found in the complexes is given in Table S3 in the Supporting Information.

^1H NMR Spectroscopy. In ^1H NMR spectra of the nanocomplexes, $[\text{UO}_2(\text{salbz})(\text{MeOH})]$, $[\text{UO}_2(5\text{-Brsalbz})(\text{MeOH})]$, and $[\text{UO}_2(5\text{-Clalbz})(\text{MeOH})]$, a significant shift in the imine $\text{CH}=\text{N}$ proton was observed between the free ligands (8.35–8.58 ppm) and nanometal complexes (9.27–9.57 ppm), indicating involvement of the lone pairs on nitrogen with the metal center. Because of the asymmetric structure of ligands and complexes, two separated signals were observed for imine protons. CH_2 protons were observed at about 4.92 ppm in the Schiff bases and about 5.33 ppm in the complexes; a significant shift was observed. The proton chemical shifts of the coordinated PBu_3 in the kinetic product appear at $\delta = 0.8\text{--}1.6$ ppm. These results were in agreement with the previous results observed for metal complexes with tributylphosphine as a ligand [9,10]. All ^1H NMR of the complexes were recorded in the $\text{DMSO-}d_6$ solvent, which repels methanol from the coordination sphere, and itself was coordinated to the uranium. Peaks due to repelled-free MeOH were observed in the ^1H NMR as a quartet at

about 4.12 ppm related to OH and a doublet at about 3.15 ppm related to CH_3 .

FTIR Spectroscopy. In the IR spectra of the nanocomplexes, $[\text{UO}_2(\text{salbz})(\text{MeOH})]$, $[\text{UO}_2(5\text{-Brsalbz})(\text{MeOH})]$, and $[\text{UO}_2(5\text{-Clalbz})(\text{MeOH})]$, a strong peak around 1580, 1612 cm^{-1} (free ligands around 1604, 1633 cm^{-1}) indicated the coordinated imine nitrogen. The asymmetric structure of ligands and complexes caused vibration of imines at two different frequencies.

Vibrational bands in the region $3423\text{--}3456\text{ cm}^{-1}$ for the ligands were assigned to the vibrations of O–H groups. It was expected that these bands should disappear in the complexes due to the coordination of oxygens to the uranium, but they persisted indicating the presence of MeOH in the complexes. The strong band close to $894\text{--}906\text{ cm}^{-1}$ was characteristic of linear uranyl ($\text{O}=\text{U}=\text{O}$) in the complexes. The weak bands at $2800\text{--}3200\text{ cm}^{-1}$ were assigned to C–H stretching vibrations. These bands, in $[\text{UO}_2(5\text{-Brsalbz})(\text{PBu}_3)]$ as a kinetic product, were stronger due to the coordination of PBu_3 .

UV–Vis Spectra. The electronic spectra plotted in wavelength (nm) of ligands and their nanocomplexes in acetonitrile were used to examine the spectral features of the U(VI) nanocomplexes in the UV–vis region from the viewpoint of energy (Fig. 4). The electronic spectra of the ligands presented three intense bands. The first band at higher energy was attributed to $\pi \rightarrow \pi^*$ transition of the phenyl ring, and the band at lower energy arose from $\pi \rightarrow \pi^*$ transition of the azomethine chromophore. The farthest energy band was $n \rightarrow \pi^*$ transition involving the promotion of the lone pair

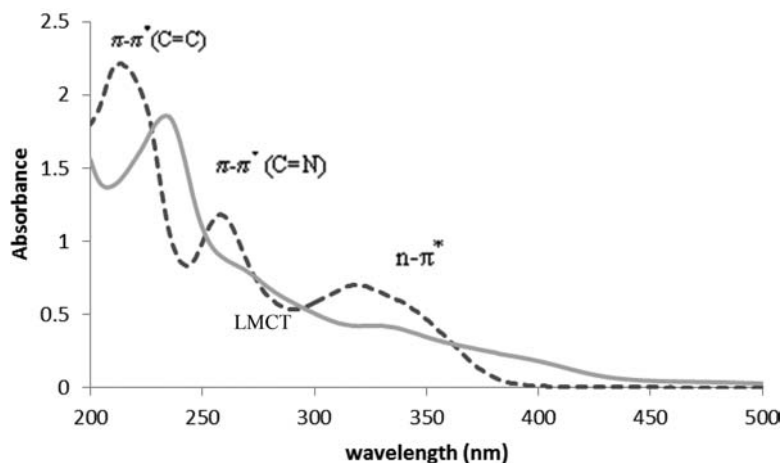


Figure 4 Electronic spectra of salbz (1.5×10^{-5} M) (dash line) and nano $[\text{UO}_2(\text{salbz})(\text{CH}_3\text{CN})]$ (4.5×10^{-5} M) (solid line) in acetonitrile.

Table II Results of Thermal Decomposition of Uranyl Schiff Base Complexes

Complex (F.W.)	(Weight Loss%) Calcd. (Found)	Temperature Range in TG (°C)	DTA (Peak) Endo/Exo	Decomposition Assignment
[UO ₂ (salbz)(MeOH)]·H ₂ O (630.22)	2.85 (3)	Under 160	Endo	Loss of H ₂ O
	5.1 (5)	160–220	Endo	Loss of MeOH
	16.5(16)	320–420	Exo	Loss of C ₆ H ₇ N
	79.9(76)	T > 420		Loss of UO ₂ C ₁₅ H ₉ O ₄ N
[UO ₂ (5-Brsalbz)(MeOH)]·H ₂ O (788.02)	2.3 (2.3)	Under 80	Endo	Loss of H ₂ O
	4.2 (3.8)	80–270	Endo	Loss of MeOH
	15.3(16)	270–400	Exo	Loss of C ₇ H ₆ N ₂
	78.2(78)	T > 400	Exo	Loss of UO ₂ C ₁₄ H ₈ O ₄
[UO ₂ (5-Brsalbz)(CH ₃ CN)] (797.02)	5.26(4.2)	Under 320	Endo	Loss of CH ₃ CN
	15.6(15)	320–380	Endo	Loss of C ₇ H ₆ N ₂
	81(80.8)	T > 380	Exo	Loss of C ₁₂ H ₆ N ₂ O ₄ Br ₂ U

electrons of the nitrogen atom to the antibonding π^* orbital. Usually $n \rightarrow \pi^*$ transition involving nitrogen atoms occurred at lower energies.

Because of the strong intensity of the characteristic absorption bands of the complexes, these absorption bands could be assigned to an electronic dipole-allowed transition arising from the coordinating ligand and/or from charge transfer between the ligand and uranium atom. Owing to the presence of the phenolate group, these ligands could act as electron donors. Since uranyl complexes contained U(VI) with an empty valence shell, the metal center was only capable of functioning as an acceptor moiety for LMCT (ligand to metal charge transfer) transition. It seemed that charge transfer band (LMCT) from oxide (=O) to uranyl occurred at lower frequencies (higher wavelengths) than the one for the transfer Schiff base²⁻ \rightarrow U(VI) [11].

Thermal Analysis. TG data of the nanocomplexes, [UO₂(salbz)(MeOH)] and [UO₂(5-Brsalbz)(MeOH)], have been studied to proof the existence of an associated water or solvent molecules either coordinated to the metal center or located freely in the crystal lattice. In thermal analysis, heating rates were suitably controlled at 20°C min⁻¹ under nitrogen atmosphere, and the weight loss was measured from the ambient temperature up to 1000°C. TG analysis for [UO₂(salbz)(MeOH)] and [UO₂(5-Brsalbz)(MeOH)] (Fig. S2 in the Supporting Information) showed two stages in the range of 30–270°C. The first stage at about 30–160°C corresponded to the loss of one hydrated water molecule. The second stage at about 100–270°C occurred due to the loss of coordinated methanol. For the complex syn-

thesized in acetonitrile, in [UO₂(5-Brsalbz)(CH₃CN)] the first stage corresponds to the loss of acetonitrile under 320°C. All thermal data are collected in Table II.

The Kinetic Aspects of Thermal Decomposition.

All the well-defined stages of DTG curves were selected to study the kinetics of decomposition of the complexes. The kinetic parameters (the activation energy E^* and the preexponential factor A^*) were calculated using the Coats–Redfern equation (1) [12]:

$$\log \left[\frac{-\log(1-a)}{T^2} \right] = \log \frac{AR}{\beta E} \left[1 - \frac{2RT}{E} \right] - \frac{E}{2.303RT} \quad (1)$$

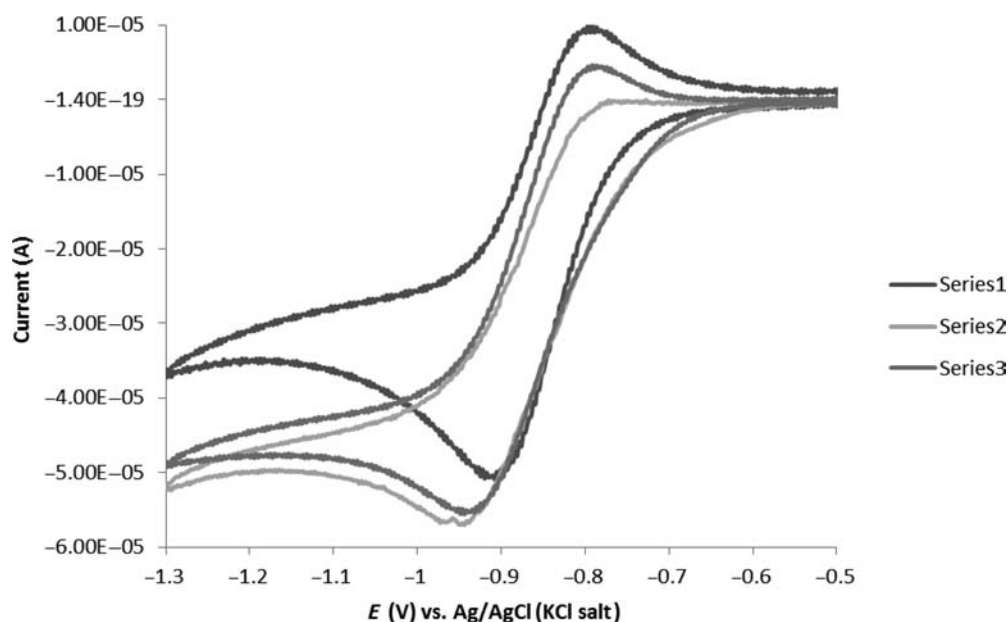
where $a = \frac{(w_0-w_t)}{(w_0-w_f)}$, w_0 the initial mass of the sample, w_t is the mass of the sample at temperature T , w_f is the final mass at a temperature at which the mass loss is approximately unchanged, β is the heating rate, and R is the gas constant. Plots of left-hand side of Eq. (1) against $1/T$ gave a straight line, in which slope and intercept were used to calculate the kinetic parameters. The goodness of fit was checked by calculating the correlation coefficient. Other systems and their steps showed the same trend.

The entropy of activation S^* was calculated using Eq. (2):

$$A^* = \frac{KT_s}{h} e^{S^*/T} \quad (2)$$

Table III Thermal and Kinetic Parameters for the Uranyl Complexes

Compound	ΔT (°C) ^a	E^* (kJ mol ⁻¹)	A^* (s ⁻¹)	S^* (J mol ⁻¹ K ⁻¹)	H^* (kJ mol ⁻¹)	G^* (kJ mol ⁻¹)
[UO ₂ (salbz)(MeOH)]	under 160	30.18	9,592	-171.26	26.79	23.03
	320–420	18.70	119.97	-211.28	13.49	74.54
[UO ₂ (5-Brsalbz)(MeOH)]	320–380	61.97	581,050.2	-140.77	56.74	50.13

**Figure 5** Cyclic voltammograms of uranyl complexes (4.5×10^{-5} M) in acetonitrile at room temperature. Scan rate: 100 mV/s. 1: Cl, 2: Br, 3: H.

where k , h , and T_s are the Boltzmann constant, the Planck constant, and the peak temperature, respectively. The enthalpy and free energy of activation were calculated using Eqs. (3) and (4) [13, 14]

$$E^* = H^* + RT \quad (3)$$

$$G^* = H^* - TS^* \quad (4)$$

Kinetic parameters for all complexes are collected in Table III.

A typical linear plot of left-hand side of the Coats–Redfern equation versus $1/T$ is shown in Fig. S3 in the Supporting Information.

The negative values of entropy of activation indicated that the activated complex had a more ordered structure than the reactants [14]. According

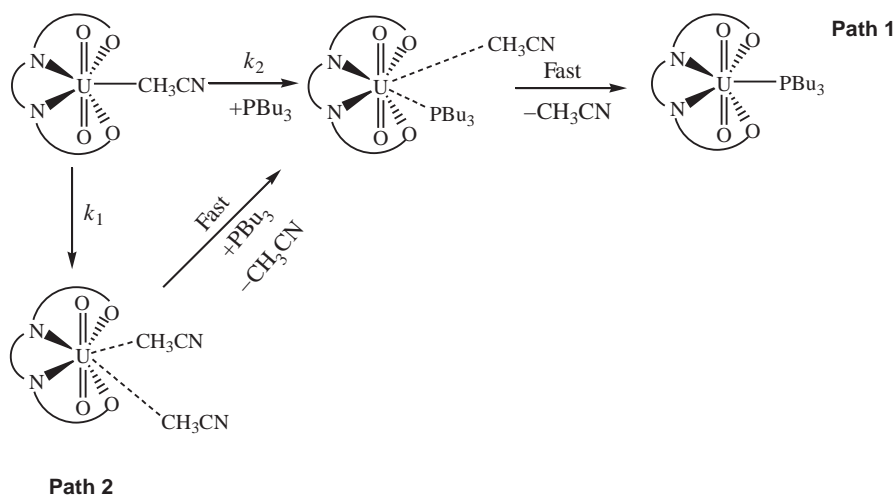
to Coats–Redfern plots (Fig. S3 in the Supporting Information), the kinetics of thermal decomposition of the studied complexes was first order in all stages.

The Electrochemical Study of Uranyl Complexes.

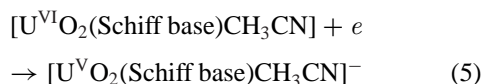
To investigate the effect of substitutional groups of the Schiff base ligands on the oxidation and reduction potential of [UO₂(Schiff base)(CH₃CN)], uranyl Schiff base complexes in the nanoform were dissolved and studied by the CV method. CV measurements for uranyl complex solutions in acetonitrile (1×10^{-3} M) and TBAP (0.10 M) as the supporting electrolyte were carried out at room temperature and in the potential range from -0.65 to -1.28 V at the scan rate $V = 0.1$ V/s. A typical cyclic voltammograms of [UO₂(Schiff base)(CH₃CN)] in the potential range from 0.0 to -1.3 V (vs. Ag/AgCl) is shown in Fig. 5. [UO₂(Schiff base)(CH₃CN)] was reduced to the mono anion [UO₂(L)(CH₃CN)]⁻ in a quasi-reversible one

Table IV Redox Potential Data of Uranyl Schiff Base Complexes in the Acetonitrile Solution

Compound	E_{pa} (V \rightarrow VI)	E_{pc} (VI \rightarrow V)	$E_{1/2}$ (VI \leftrightarrow V)
[UO ₂ (salbz)(MeOH)]	-0.7864	-0.9583	-0.8724
[UO ₂ (5-BrSalbz)(MeOH)]	-0.7938	-0.9485	-0.8711
[UO ₂ (5-ClSalbz)(MeOH)]	-0.7913	-0.9173	-0.8543

**Scheme 1**

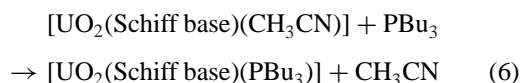
electron step (Eq. (5)).



Upon the reversal of the scan direction, the U(V) complex was oxidized to U(VI) at over potentials. The oxidation potentials for the different complexes are collected in Table IV. The formal potentials ($E_{1/2}(\text{VI} \leftrightarrow \text{V})$) for the U(V/VI) redox couple were calculated as the average of the cathodic (E_{pc}) and anodic (E_{pa}) peak potentials of this process.

The cathodic peak potentials increased in the order of $\text{H} < \text{Br} < \text{Cl}$. Chloride and Bromide groups on the para position (5-Br and 5-Cl) acted as an electron-withdrawing groups. This factor accelerated reduction of 5-Br and 5-Cl related to 5-H.

Kinetic Study of the Exchange of Solvent with PBu_3 on the Uranyl Complexes. The kinetics of the interaction between the nano uranyl Schiff base complexes as an acceptor and PBu_3 as a donor was studied (Eq. (6)).



By dissolving the complexes in acetonitrile, methanol was exchanged with acetonitrile, thus acetonitrile occupied the fifth position in the equatorial plane.

Plots of k_{obs} versus $[\text{PBu}_3]$ exhibited a nonzero intercept. Thus the rate law for the reaction is as follows (Eqs. (7) and (9))

$$R = \{k_1 + k_2[\text{PBu}_3]\}[\text{complex}] \quad (7)$$

under the pseudo-first-order condition:

$$R = k_{\text{obs}}[\text{complex}] \quad (8)$$

where

$$k_{\text{obs}} = k_1 + k_2[\text{PBu}_3] \quad (9)$$

k_2 is the second-order rate constant (Scheme 1, Path 1) and k_1 is the first-order rate constant (Scheme 1, Path 2).

The rate constants and the activation parameters are collected in Tables V, VI and S4–S6 in the Supporting

Table V $10^1 k_1^a$ (s^{-1}), $10^{-2} k_2^a$ ($M^{-1} s^{-1}$) for the Reaction of Complexes with PBu_3 at Different Temperatures

Temperature ($^{\circ}C$)	[UO ₂ (salbz)(CH ₃ CN)]		[UO ₂ (5-Cl ₂ salbz)(CH ₃ CN)]		[UO ₂ (5-Brsalbz)(CH ₃ CN)]	
	k_1 (s^{-1})	k_2 ($M^{-1} s^{-1}$)	k_1 (s^{-1})	k_2 ($M^{-1} s^{-1}$)	k_1 (s^{-1})	k_2 ($M^{-1} s^{-1}$)
10	5.1 (0.1)	0.4 (0.1)	6.6 (0.2)	5.8 (0.1)	5.1 (0.1)	3.6 (0.1)
20	2.2 (0.1)	0.7 (0.1)	0.4 (0.1)	8.6 (0.2)	9.7 (0.1)	4.2 (0.1)
30	1.7 (0.2)	0.8 (0.2)	2.9 (0.1)	10.7 (0.1)	2.9 (0.1)	4.5 (0.2)
40	2.6 (0.3)	0.9 (0.2)	5.6 (0.1)	13.1 (0.2)	3.8 (0.1)	5.5 (0.3)

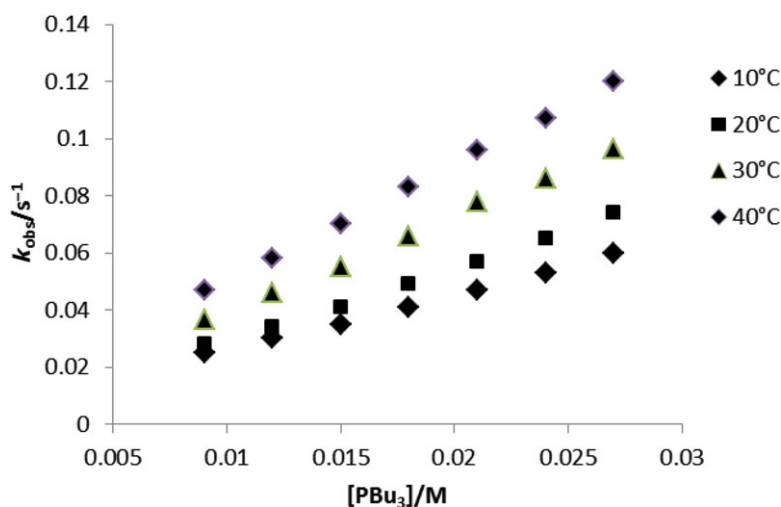
^aThe numbers in parentheses are the standard deviations of k .

Table VI Activation Parameters $\Delta H^{\ddagger a}$, $\Delta S^{\ddagger a}$, and $\Delta G^{\ddagger b}$ for the Interaction of the Complexes with PBu_3

Complex	ΔH^{\ddagger} ($kJ mol^{-1}$)	ΔS^{\ddagger} ($J K^{-1} mol^{-1}$)	ΔG^{\ddagger} ($kJ mol^{-1}$)
Nano-[UO ₂ (5-Cl ₂ salbz)(MeOH)]	17.1 (2.0)	-130.9 (6.6)	58.1 (2.9)
Nano-[UO ₂ (5-Brsalbz)(MeOH)]	7.1 (1.4)	-171.2 (4.8)	60.7 (2.1)
Nano-[UO ₂ (salbz)(MeOH)]	17.1 (5.2)	-152.9 (17.5)	64.9 (7.5)

^aThe numbers in parentheses are the standard deviations.

^b ΔG^{\ddagger} was calculated at $T = 40^{\circ}C$.

**Figure 6** Plots of k_{obs} versus $[PBu_3]$ for [UO₂(5-Cl₂salbz)(CH₃CN)] at different temperatures (10–40 $^{\circ}C$).

Information. The mechanism as shown in Scheme 1 was suggested for the reaction of uranyl complexes with PBu_3 .

Two paths were suggested for the reaction. In Path 1, PBu_3 was added to the uranium center by an associative mechanism with a rate constant k_2 , with the suggested structures shown in Scheme 1. An octacoordinate intermediate was formed and then by repelling the solvent molecule a heptacoordinate product reappeared. In Path 2 (a dissociative path) with the k_1 rate constant, a hexacoordinate intermediate was formed and PBu_3 was coordinated to the uranium center in a fast step.

The k_2 values were obtained from the slope of the linear plots of k_{obs} versus the donor concentration $[PBu_3]$, and the k_1 values were obtained from their intercept (Fig. 6).

The activation parameters of the studied systems were calculated by using the Eyring equation (10):

$$\ln(k_2/T) = -\Delta H^{\ddagger}/RT + \Delta S^{\ddagger}/R + 23.8 \quad (10)$$

A typical linear Eyring plot of $\ln(k_2/T)$ versus $1/T$ with a good correlation of 0.97–0.99 at four different temperatures for [UO₂(5-Cl₂salbz)(CH₃CN)] is shown

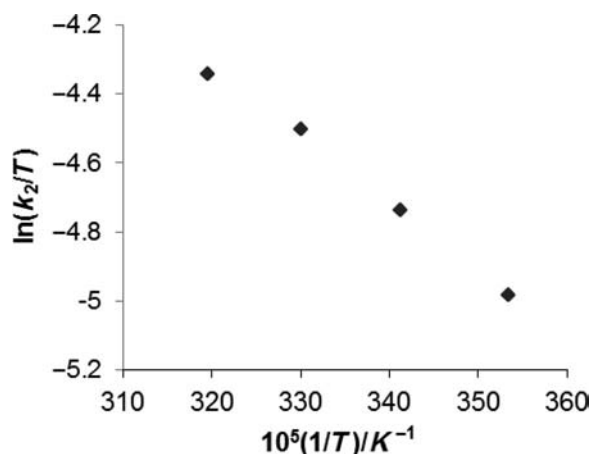


Figure 7 Linear plot for $\ln(k_2/T)$ against $1/T$ for $[\text{UO}_2(5\text{-Clalpbz})(\text{CH}_3\text{CN})]$.

in Fig. 7. Also, the ΔG^\ddagger values were calculated using the equation $\Delta G^\ddagger = \Delta H^\ddagger - T\Delta S^\ddagger$ at $T = 313$ K.

The k_2 values for the ligands entry showed high span, suggesting the dependence of the rate constant on the nature of the complex. The low ΔH^\ddagger values and the large negative ΔS^\ddagger values were compatible with an associative (A) mechanism. For studying the effect of substitutional groups, we compared the complexes, 5-Br, 5-Cl, and salbz, so that complexes differ in the electronic properties; the smallest k_2 values were found for $[\text{UO}_2(\text{salbz})(\text{CH}_3\text{CN})]$, whereas the highest values existed for $[\text{UO}_2(5\text{-Clalpyr})(\text{CH}_3\text{CN})]$ because of the electron-withdrawing groups on the aromatic ring. It was clear that the existence of the bromo and chloro groups made the Schiff base complexes better acceptors.

It was concluded that the electronic effect took part during the substitution reaction. The following trend of rate constant was obtained: $\text{UO}_2(5\text{-Clalpyr}) > \text{UO}_2(5\text{-Brsalpyr}) > \text{UO}_2(\text{salpyr})$.

Anticancer Activity. Anticancer activity of $[\text{UO}_2(\text{salbz})(\text{MeOH})]$ and $[\text{UO}_2(5\text{-Clalbz})(\text{MeOH})]$ complexes was tested on *the Aspergillus* fungus. Details of the experiment are presented below.

Cell Culture and MTT Assay for Analysis of Anticancer Properties of the Complexes. The cancer cell lines were cultured in RPMI 1640 medium (HiMedia, Mumbai, India) supplemented with 10% fetal calf serum (Biochrom, Berlin, Germany). 100 IU/mL of penicillin and 100 mg/mL of streptomycin were also added to the media as antibiotics to control the growth of contaminating microorganisms. The cells were cultured in 96-well tissue cul-

ture plates (Greiner) and kept at 37°C in a humidified atmosphere of 5% CO_2 in a CO_2 incubator. All the experiments were performed using cancer cell line (Jurkat) of 10–15 passage. The growth inhibitory effect of uranyl complexes toward the cancer cells was measured using the 3-(4,5-dimethylthiazol-2-yl)-2,5-diphenyltetrazolium bromide (MTT) assay. Briefly, the cleavage and conversion of the soluble yellowish MTT to the insoluble purple formazan by active mitochondrial dehydrogenase of living cells has been used to develop an assay system alternative to other assays for the measurement of cell proliferation. The drug treatment performed as the harvested cells was seeded in to a 96-well plate (2.5×10^4 cell/well) with varying concentrations of the sterilized uranyl complexes (0–100 μM) and incubated for 24 and 48 h. Four hours to the end of incubations, 25 μL of the MTT solution (5 mg/ml in PBS) was added to each well containing fresh and cultured medium. At the end, the insoluble formazan was produced and it was dissolved in a solution containing 10% SDS and 50% DMF (left for 1 h at 37°C in dark conditions) and optical density (OD) was read against a reagent blank with a multiwell scanning spectrophotometer (ELISA reader; Bio-Tek's ELx808, Winooski, VT) at a wavelength of 570 nm. The absorbance was a function of the concentration of a converted dye. The OD value of study groups was divided by the OD value of untreated control and presented as a percentage of control (as 100%). Also the values of IC50 (the concentrations required for 50% growth inhibition), after 24 h of incubation with the complexes, were calculated.

According to Table VII and Fig. 8, $[\text{UO}_2(\text{salbz})(\text{MeOH})]$ did not show anticancer activity, whereas $[\text{UO}_2(5\text{-Clalbz})(\text{MeOH})]$ in 50–100 μM was able to kill about 60–70% of the cancer cell.

CONCLUSIONS

This study involved the synthesis of crystalline and nanoforms of uranyl unsymmetrical Schiff base complexes. The preliminary TG and IR measurements confirmed the same behavior of both forms. The kinetics and mechanism of solvent substitution reactions with

Table VII IC50 Values (Mm/mL) of the Complexes against Jurkat Cell Line

Complex	IC ₅₀
$[\text{UO}_2(\text{salbz})(\text{MeOH})]$	–
$[\text{UO}_2(5\text{-Clalbz})(\text{MeOH})]$	45.8

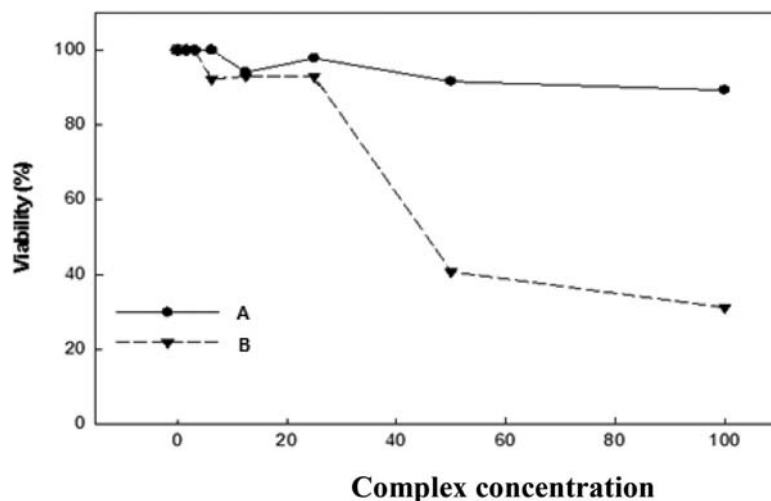


Figure 8 Viability (%) versus the complex concentration. All the experiments were performed using cancer cell line (Jurkat) of 10–15 passage.

tributylphosphine was investigated in acetonitrile spectrophotometrically. The uranium in $U^{VI}O_2^{2+}$ has no 4f electron and acted as an acceptor, whereas PBu_3 acted as a donor and replaced the weakly coordinated solvent. The high span of the rate constant (k_2) as well as low ΔH^\ddagger and large negative ΔS^\ddagger value suggested an associative (A) mechanism. The electronic effect was important for the rate of the substitution reaction. The trend of k_2 values showed that electron-withdrawing substitutional groups such as Cl and Br to the phenolic oxygen of the Schiff base accelerated the substitution reaction by attracting PBu_3 as an electron donor toward the uranium center.

CV was used to investigate the effect of the substitutional group of ligands on the reduction and oxidation of uranium $U^{(VI)} \leftrightarrow U^{(V)}$. Again, electron-withdrawing substitutional groups accelerated the reduction of uranium.

The kinetics of the thermal decomposition was investigated. Kinetic parameters (the activation energy E^* and the preexponential factor A^*) were reported, and the negative values of the entropy of activation showed that the activated complex had a more ordered structure than the reactants. According to Coats–Redfern plots, the kinetics of the thermal decomposition of the studied complexes was of the first order in all stages.

By evaluating the X-ray structures of the complexes, it was found that one solvent molecule coordinated weakly to the uranium center. This was also confirmed by TG studies.

The project P204/11/0809 of the grant agency of the Czech Republic supported the crystallographic part of the work.

BIBLIOGRAPHY

- Comini, E. *Anal Chim Acta* 2006, 568, 28–40.
- Kocak, N.; Sahin, M.; Kucukkolbasi, S.; Ozden Erdogan, Z. *Int J Biol Macromolec* 2012, 51, 1159–1166.
- Karlsson, H. L.; Gustafsson, J.; Cronholm, P.; Moller, L. *Toxicol Lett* 2009, 188, 112–118.
- Tamami, B.; Ghasemi, S. *Appl Catal A* 2011, 393, 242–250.
- Agilent Technologies, *Crys Alis PRO*; Yarnton: Oxfordshire, UK, 2012.
- Palatinus, L.; Chapuis, G. *J. Appl Cryst* 2007, 40, 786–790.
- Petricek, V.; Dusek, M.; Palatinus, L. *Jana 2006*; Structure Determination Software Programs; Institute of Physics: Praha, Czech Republic, 2006.
- Takao, K.; Ikeda, Y. *Inorg Chem* 2007, 46, 1550–1562.
- Anthonyamy, A.; Balasubramanian, S. *Inorg Chem Commun* 2005, 8, 908–911.
- Kumar, D. N.; Garg, B. S. *Spectrochim Acta, Part A* 2006, 59, 141–147.
- Bharara, M. S.; Strawbridge, K.; Vilsek, J. Z.; Bray, T. H.; Gorden, A. E. V. *Inorg Chem* 2007, 46, 8309–8315.
- Coats, A. W.; Redfern, J. P. *Nature* 1964, 201, 68–69.
- Aravindakshan, K. K.; Muraleedharan, K. *Thermochim Acta* 1989, 155, 247–253.
- Nair, M. K. M.; Radhakrishnan, P. K. *Thermochim Acta* 1995, 261, 141–149.